Radiation Protection Dosimetry (2019), Vol. 185, No. 1, pp. 42–49
Advance Access publication 12 January 2018
doi:10 1093/rpd/ncy214

A SIMPLIFIED METHOD FOR THE WATER-EQUIVALENT DIAMETER CALCULATION TO ESTIMATE PATIENT DOSE IN CT EXAMINATIONS

Choirul Anam[1,*], Idam Arif[2], Freddy Haryanto[2], Rena Widita[2], Fauzia P. Lestari[2], Kusworo Adi[1] and Geoff Dougherty[3]
[1]Department of Physics, Faculty of Mathematics and Natural Sciences, Diponegoro University, Jl. Prof. Soedarto SH, Semarang 50275, Central Java, Indonesia
[2]Department of Physics, Faculty of Mathematics and Natural Sciences, Bandung Institute of Technology, Ganesha 10, Bandung 40132, West Java, Indonesia
[3]Department of Applied Physics and Medical Imaging, California State University Channel Islands, Camarillo, CA 93012, USA

*Corresponding author: anam@fisika.undip.ac.id

Received 12 September 2018; revised 8 November 2018; editorial decision 8 November 2018; accepted 9 November 2018

We proposed and evaluated a water-equivalent diameter calculation without using a region of interest (ROI), ($D_{w,t}$) and compared it with the results of using a ROI fitted to the patient border ($D_{w,f}$). Evaluations were carried out on thoracic and head CT images. We found that the difference between $D_{w,t}$ and $D_{w,f}$ was within 5% for all images in the head region, and most images were within 5% (27 of the 30 patients, 90%) in the thoracic region. We also proposed a method to automatically detect and eliminate the patient table (or head support) from images and evaluated the water-equivalent diameter values after the table had been removed ($D_{w,nt}$). This method was able to recognize and remove the patient table from all images used. By removing the table, the water-equivalent diameter ($D_{w,nt}$) became more accurate and the difference from $D_{w,f}$ was within 5% for all images (head and thoracic images).

INTRODUCTION

Several studies have reported that CT examinations result in a potential risk for future cancer occurrence[1–3], especially in pediatric patients due to their more radiosensitive cells and their long life expectancy. The risk is generally considered small compared to the benefits gained from CT, but this risk cannot be ignored[4, 5] especially given the increasing use of CT scans in various countries[5, 6]. The risk of cancer is reported to increase with increasing radiation dose. Accurate estimation of radiation dose is very important in order to estimate and minimize the risk experienced by patients. The dose optimization process should be used to reduce the dose as low as possible while maintaining image quality to diagnose the abnormalities[7].

Accurate dose estimates in patients must consider two main aspects, namely the CT output dose and the patient's specific condition[8, 9]. The metric used for estimating the CT output dose is the volume CT dose index ($CTDI_{vol}$)[10], which is affected by almost all CT input parameters such as kVp, mAs, pitch, beam width and type of filter[11]. The patient's specific condition can be determined by the geometrical size or/and the radiological size[12, 13]. The geometrical size can be represented by a diameter in the lateral direction or in the transverse direction or in a combination of the two or using the effective diameter (D_{eff})[14–16]. The radiological size takes into account the geometrical size and attenuation of the scanned body and it can be represented using a water-equivalent diameter (D_w)[17, 18]. The characterization of the patient using D_w is preferred and more accurate than using only geometrical quantities (D_{eff}, LAT or AP)[19, 20]. AAPM has recommended the use of D_w[21] as an improvement from the use of D_{eff}[22]. The combination of the CT output dose and the specific condition of this patient is used to estimate the dose received by the patient in a metric known as the size-specific dose estimate (SSDE)[23–25].

The calculation of D_w using an axial image is considered more accurate than using a localizer radiograph because the D_w calculation is not affected by image magnification[26], as is often the case with the localizer radiograph due to mis-centering. In addition, the value of each pixel of the axial image has been calibrated in Hounsfield units (HU), which can be used directly to calculate D_w[27]. This is different from using the localizer radiograph where the pixel values must be calibrated first before they can be used to calculate D_w[20, 24].

There are two approaches commonly used for D_w calculations using axial images. One uses a circular

region of interest (ROI) to include all the relevant parts of the patient and exclude everything else[27], before calculating D_w. A second approach uses a ROI that is fitted to the contour of the patient[28]. This latter approach is considered more accurate but making a fitted ROI to a patient border manually may not be easy and takes a relatively long time, so it can be impractical for a busy CT center. Instead, the fitted ROI can be found automatically[13]. Anam *et al.*[29] compared the two approaches to images of the head, chest, abdomen and pelvis. The results showed that the two approaches did not differ significantly in the images of the head, abdomen and pelvis, but in the thorax images there were significant differences. However, the evaluation was carried out only on CT dedicated to radiotherapy using a flat table[29]. To date, comparison of the two approaches on standard CT in radiology with a non-flat table has not been done.

In principle, the D_w calculation could be carried out using the entire image area, without a ROI. This approach is hypothesized to be relatively accurate if there are no objects with relatively large attenuation in the image, such as the patient table, which would cause an increase in the D_w values. This study evaluated the D_w calculation using this simplified, practical approach. We compared the results with the D_w calculated using the fitted ROI which is considered the gold standard and using a circular ROI. To broaden the usefulness, we proposed a method to automatically detect and eliminate patient tables (or head supports) from axial images and compared D_w values after the patient table (or head support) had been removed from the image. Evaluations were carried out on two types of examinations, namely thoracic and head CT taken in a radiology department, rather than in a radiotherapy department for a treatment planning system.

METHODS

D_w calculation

AAPM No. 220 suggested that the D_w calculation was carried out by making a circular ROI around patients as shown in Figure 1a. Following this approach, D_w was designated as $D_{w,c}$ and its value calculated using the following equation:

$$D_{w,c} = 2\sqrt{\left[\frac{1}{1000}\overline{\mathrm{HU}_c} + 1\right]\frac{A_c}{\pi}} \quad (1)$$

$\overline{\mathrm{HU}_c}$ was the average of Hounsfield unit within the circular ROI of area A_c.

D_w was also calculated using a ROI fitted to the contour of the patient as shown in Figure 1b. In this approach, D_w was designated as $D_{w,f}$ and calculated using the following equation:

$$D_{w,f} = 2\sqrt{\left[\frac{1}{1000}\overline{HU_f} + 1\right]\frac{A_f}{\pi}} \quad (2)$$

$\overline{HU_f}$ was the average of Hounsfield unit within the fitted ROI and of area A_f. In this study, $D_{w,f}$ was used as the reference and other approaches were compared with it. $D_{w,f}$ was calculated automatically using the algorithm proposed previously[13]. This automatic $D_{w,f}$ calculation method has been validated and gives the same results as the manual calculation within 0.5%[13].

In the current study, the calculation of D_w was carried out directly with the whole image, without requiring a ROI. This simplified approach is shown in Figure 1c. In this approach, D_w has been designated as $D_{w,t}$ and calculated using the following equation:

$$D_{w,t} = 2\sqrt{\left[\frac{1}{1000}\overline{HU_t} + 1\right]\frac{A_t}{\pi}} \quad (3)$$

With this approach, the area used was the area of the entire image, which can easily be calculated as follows:

$$A_t = \mathrm{FOV}^2 \quad (4)$$

The field of view (FOV) can be obtained from the DICOM header, and the average HU of the entire image can be calculated by summing all pixel values and dividing by the total number of pixels:

$$\overline{\mathrm{HU}_t} = \frac{\sum_{y=1}^{n}\sum_{x=1}^{n} HU(x, y)}{n \times n} \quad (5)$$

However, this approach may be less accurate in estimating D_w if there are objects such as the patient table, patient's clothes or other objects in the image. Wang *et al.*[27] reported that the effect of the patient table can be significant, so it can be removed automatically as seen in Figure 1d. We have designated the D_w value after table removal as $D_{w,\mathrm{nt}}$.

Patient table detection

The detection of the patient table (or head support) is intended to remove any parts of the table (or head support) from the image so that the D_w calculation using the entire image is more accurate. The stages of the detection and removal of the table (or head support) are shown in Figure 2. After opening the patient image (Figure 2a), a thresholding operation was performed with a HU value of −500 (Figure 2b). The labeling operation is shown in Figure 2c. The average position of the object in the y-axis for all labeled objects is shown in Figure 2d. The average

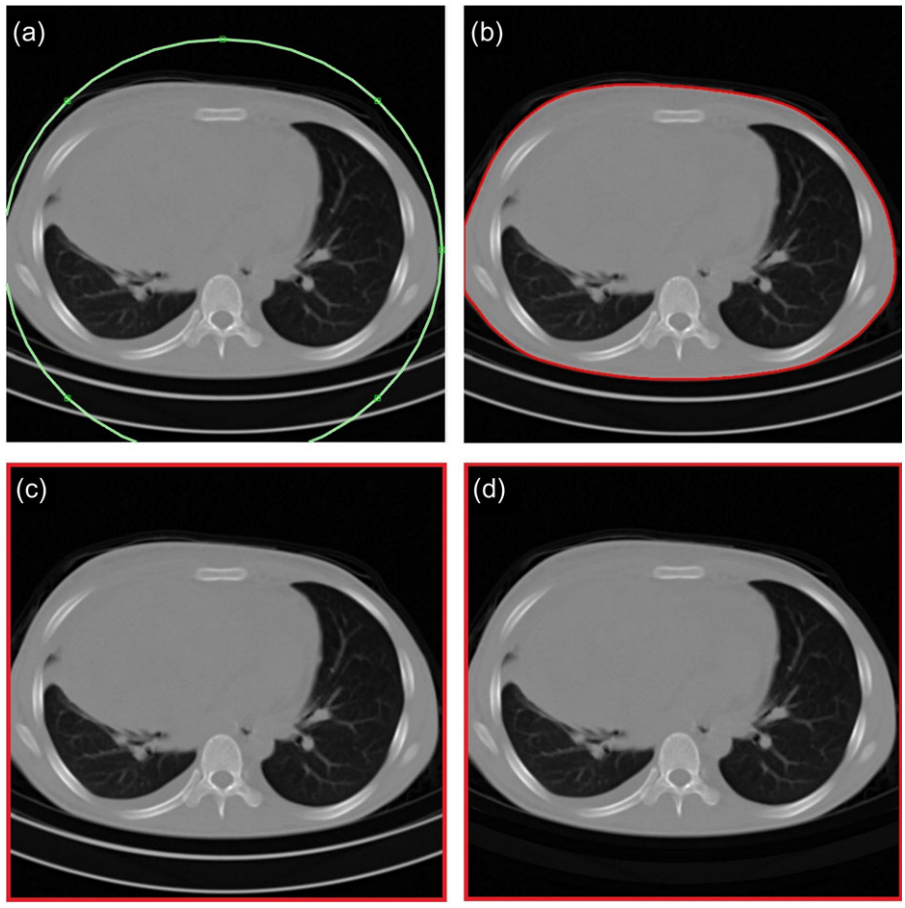

Figure 1. Different approaches to the D_w calculation. (**a**) Using a circular ROI, which covers all parts of the patient, as used in AAPM TG 220[21]. (**b**) Using a ROI fitted to the contours of the patient as proposed previously[13]. (**c**) A simplified approach without a ROI as proposed in the current study. The value of average HU and the area (A) were directly calculated from the entire image. In this approach, the patient table is still included in the calculation. (**d**) Same as method (c), but the table was removed from the image automatically.

value of this position is used to detect and remove the table (or head support). In this study, the patient table (or head support) was defined as an object with an average position on the y-axis >450 (pixels). This value limit may be set to be smaller or greater depending on the FOV used. Figure 2e shows an object with a y-axis average position >450 (pixels), viz. the patient table. The table image was then enlarged by a dilation process with a diamond-shaped structuring element of size five pixels. The patient table (or head support) can be removed from the patient's image by changing the HU value at the table position to −1000 HU, as shown in Figure 2f. The complete codes for detecting and removing the patient table (or head support) from the image can be found in the Supplementary material.

RESULTS

The result of the automated patient table removal

Our method successfully detected and removed all remnants of the patient table (or head support) automatically from all the images used in this study. In the thoracic images, the appearance of the remnants of the patient table can be classified into several types: the upper and lower parts of the table appear completely (Figure 3a), the upper table appears completely but lower parts appear partially (Figure 3b), only the upper part of the table appears completely (Figure 3c) and only a small part of the upper table appears partially (Figure 3d). In the head images, the head support only appears partially (Figure 4a) or not at all (Figure 4b). This proposed method is

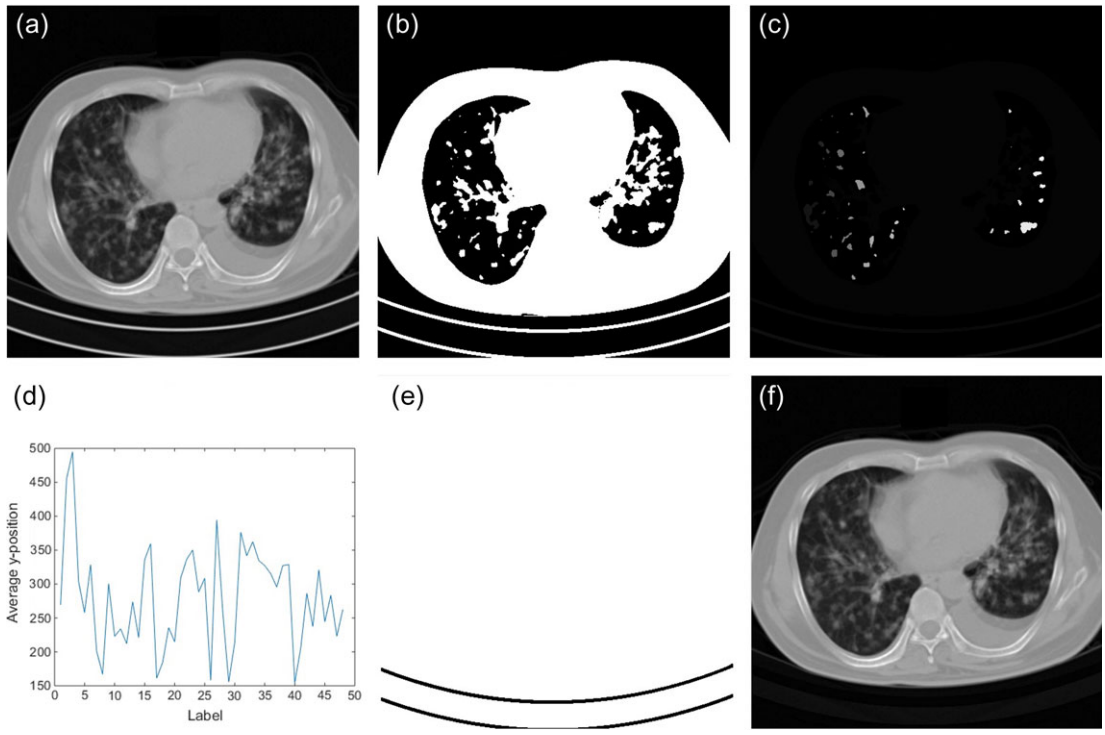

Figure 2. Steps in the detection of the patient table (or head support). (**a**) Original image, (**b**) thresholded image, (**c**) labeled image, (**d**) graph of average y-position for all labeled objects, (**e**) image of the detected table and (**f**) image of patient without table.

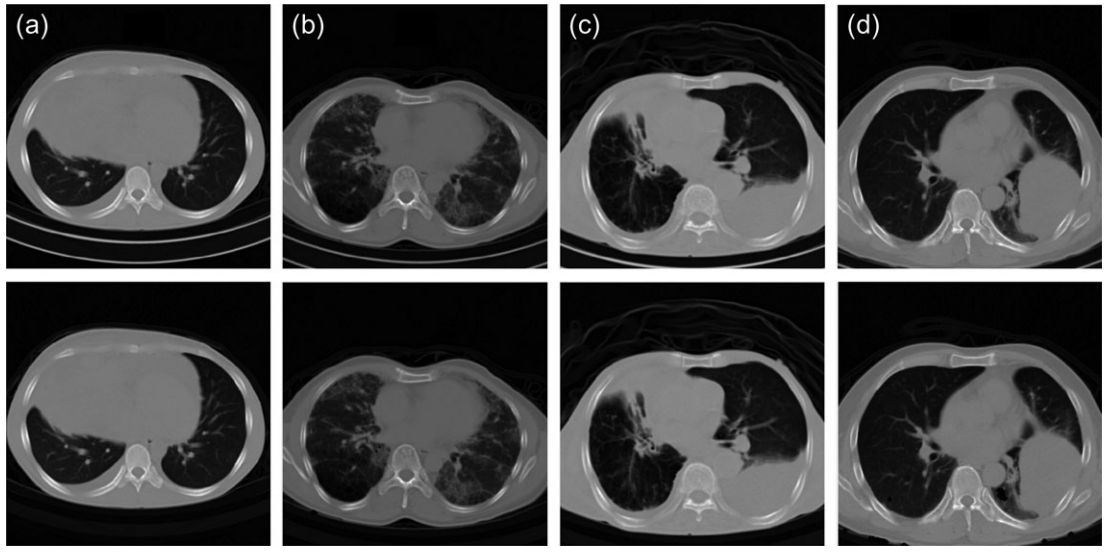

Figure 3. Appearance of the patient table in the thoracic images. The first row shows the original images and the second row shows the images after the patient table has been automatically removed. (**a**) The upper and lower parts of the table appear completely, (**b**) the upper table appears completely but lower parts appear partially, (**c**) only the upper part of the table appears completely and (**d**) only a small part of the upper table appears partially.

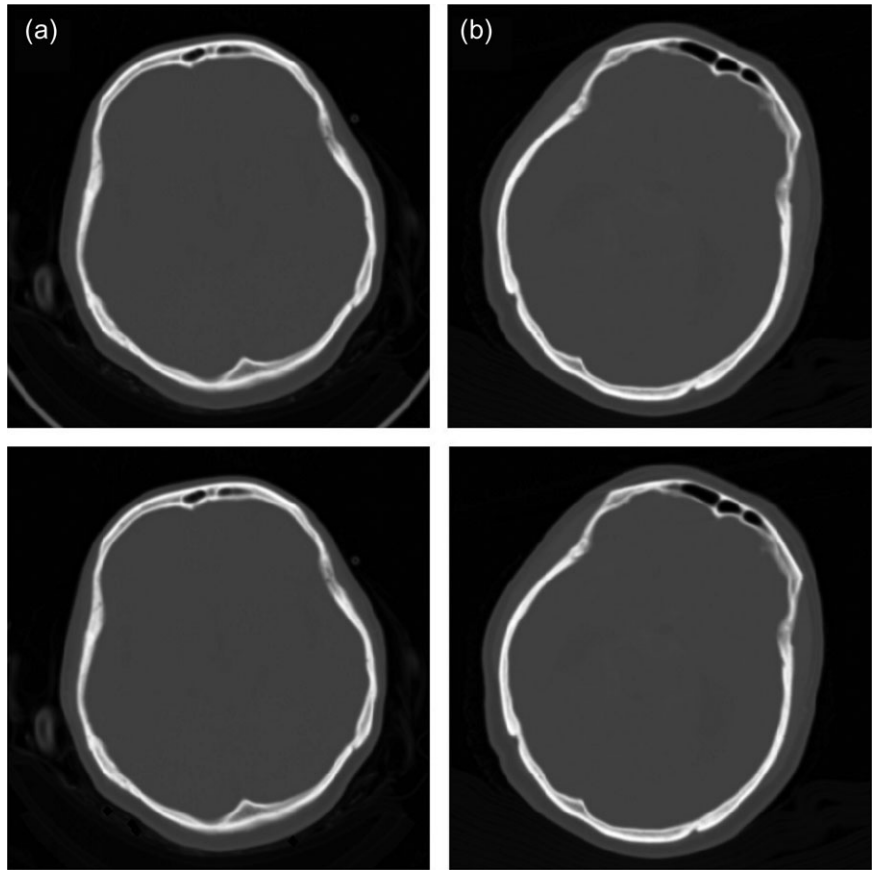

Figure 4. Appearance of the head support in the head images. The first row shows the original images, and the second row shows the images after the head support has been automatically removed. (**a**) The head support appears partially, and (**b**) the head support does not appear at all.

able to detect and remove the patient table (or head support) automatically, as shown by the second rows of the Figures 3 and 4.

The comparison of D_w values

There are four variants of D_w in this study, namely $D_{w,c}$, $D_{w,f}$, $D_{w,t}$ and $D_{w,\mathrm{nt}}$. The $D_{w,c}$ is D_w calculated using a circular ROI as described in AAPM 220, $D_{w,f}$ is D_w calculated using a ROI fitted to patient, $D_{w,t}$ is D_w calculated using the entire image without a ROI and $D_{w,\mathrm{nt}}$ is D_w calculated using the entire image without a ROI after removing the table. $D_{w,f}$ is considered the ground truth in this study.

Histogram graphs of differences in the values of $D_{w,c}$, $D_{w,t}$ and $D_{w,\mathrm{nt}}$ from $D_{w,f}$ in the thoracic images are shown in Figure 5. The difference of $D_{w,c}$ from $D_{w,f}$ is within 5%, with an average value of $1.8 \pm 0.7\%$. The percentage differences between $D_{w,t}$ and $D_{w,f}$ are <5% for most patients (27 patients or 90%), with a mean value of $3.3 \pm 1.2\%$. Meanwhile, the difference between $D_{w,\mathrm{nt}}$ and $D_{w,f}$ does not exceed 5%, with an average value of $1.4 \pm 0.5\%$. This shows that if the patient's table is removed, the $D_{w,\mathrm{nt}}$ values are more accurate than using a circular ROI ($D_{w,c}$).

The differences in the values of $D_{w,c}$, $D_{w,t}$ and $D_{w,\mathrm{nt}}$ from $D_{w,f}$ in the head images are shown in Figure 6. For the head images, the differences of $D_{w,c}$, $D_{w,\mathrm{nt}}$ and $D_{w,t}$ from $D_{w,f}$ are <5%. The difference between $D_{w,c}$ and $D_{w,f}$ is the smallest with an average of $0.8 \pm 0.6\%$.

DISCUSSION

The water-equivalent diameter calculation method proposed in this study ($D_{w,t}$) is very practical, because there is no need to make a ROI in the patient image. The area of ROI is calculated easily as the square of the FOV. We found that the value of $D_{w,t}$ calculated using this method is comparable to

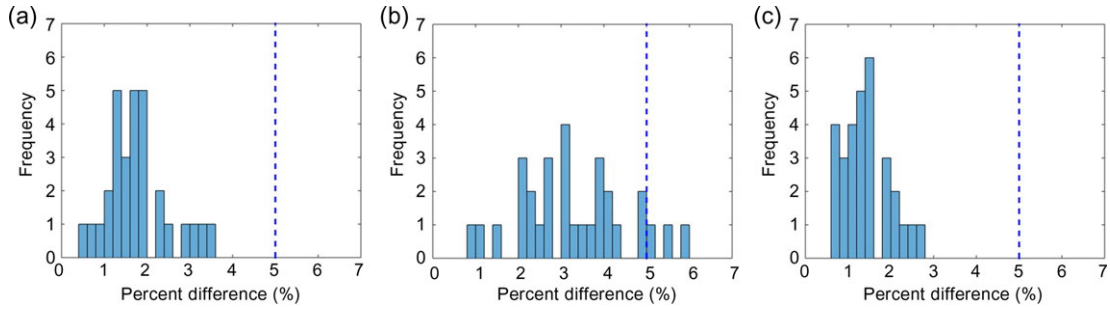

Figure 5. The histogram graphs of the percentage difference from $D_{w,f}$ in the thoracic images, for (**a**) $D_{w,c}$, (**b**) $D_{w,t}$ and (**c**) $D_{w,nt}$. The dashed line shows the 5% of difference limit.

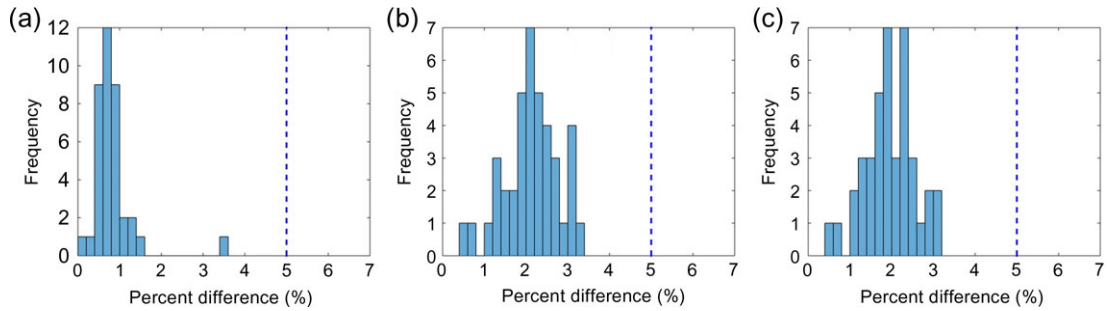

Figure 6. The histogram graphs of the percentage difference from $D_{w,f}$ in the head images, for (**a**) $D_{w,c}$, (**b**) $D_{w,t}$ and (**c**) $D_{w,nt}$. The dashed line shows the 5% of difference limit.

that using a ROI fitted to the patient border ($D_{w,f}$). In the thorax, the difference was only $3.3 \pm 1.2\%$, and in the head, it was only $2.1 \pm 0.7\%$. This shows that this method can be used in clinical applications with acceptable accuracy.

One might expect that the direct $D_{w,t}$ calculation (using the entire image without ROI) would cause the water-equivalent diameter value to be much greater compared to using a fitted ROI ($D_{w,f}$), because the value of A_{image} is much greater than the value of A_{patient}. However, when the water-equivalent diameter is calculated directly from the entire image ($D_{w,t}$), the average HU value of the image is much smaller than the average HU in the patient, because there is a lot of air outside the patient with a HU value of around −1000. Thus, a combination of an increase in A_{image} and a decrease in average HU_{image} causes the $D_{w,t}$ value not to increase significantly.

However, the $D_{w,t}$ calculation is still less accurate than the circular ROI method ($D_{w,c}$). The difference between $D_{w,c}$ and $D_{w,f}$ was $1.8 \pm 0.7\%$ in the thorax and $0.8 \pm 0.6\%$ in the head. A previous study regarding the comparison between $D_{w,c}$ and $D_{w,f}$ by Anam *et al.*[29] reported that the differences were $6.2 \pm 1.7\%$ for the thorax and $1.5 \pm 0.3\%$ for the head. The smaller difference values in the current study compared to the previous study are because the images in the earlier study were scanned using a CT dedicated to radiotherapy with a patient table made from solid wood material without a cavity in the middle of table, while the current study used a CT commonly operated within the radiology department. The patient table in the radiology department is made of carbon fiber with cavities in the middle part of table. Thus, the contribution of the table to the water-equivalent diameter in this study is smaller than in the previous study[29].

If the use of a method without any ROI is desired, more accurate results can be obtained by removing the patient table (or head support). The difference between $D_{w,nt}$ and $D_{w,f}$ in the thoracic images was then $1.4 \pm 0.5\%$ and in the head it was $2.0 \pm 0.6\%$. Compared to D_w, which was calculated using a circular ROI ($D_{w,c}$), this approach in the thoracic part was more accurate. However, in the head, $D_{w,nt}$ was less accurate than $D_{w,c}$. The difference between $D_{w,c}$ and $D_{w,f}$ in the head image was $0.8 \pm 0.6\%$.

We showed that in the chest images the use of the table removal algorithm improved the accuracy of the water-equivalent diameter value. For the head

images, the the water-equivalent diameter with head support removal ($D_{w,\mathrm{nt}}$) is no different from that without it ($D_{w,t}$); indeed only a few of our images had parts of the head support in them. However, the head support can be fully included in the image if the user sets the FOV too large or mis-centering occurs in a direction higher than the iso-center.

There are several algorithms for recognizing and removing the patient table from an image[30–32]. The table removal algorithm by Zhu *et al.*[30] cannot be carried out on axial images, so that axial images must be reformatted into sagittal plane. The assumption used is that the table in the sagittal plane is a straight line, so that it can be detected by using the Hough transform. Before the Hough transformation, thresholding and edge detection should be performed. The results of the Hough transform are displayed as a histogram and the table parts will be detected as objects with the highest accumulated values. After the table position is detected, the table pixel values are replaced by a CT value equivalent to 'air'. Zhu *et al.*[30] reported that it was able to detect patient tables from various vendors. We used the algorithm, and it could detect and remove the patient tables from all our images. The limitations of the algorithms are: first, if the table is not perpendicular to the scanner, the assumption that the table is a straight line cannot be used. However, it is not case in our images. Second, the algorithm repeats the process 512 times for every sagittal image, so it is time consuming.

In this study, we have proposed a simple method for detecting and removing the patient table from axial images, so that image reformatting is not needed. Unlike the Zhu *et al.*[30] method where the calculation must be repeated 512 times, in this method, the loops were only done as much as the number of slices used. For example, in this study, looping was only carried out 30 times, because the average number of slices were around 30. Thus, the proposed method was computationally faster. The algorithm was also able to detect the table (head support) in all the images used in this study. The limitation of the proposed method is that the patient table is determined by its position, that is the average object on the y-axis. In this case, the table is an object with a y-axis average position >450 (pixels). This assumption may not be used for images that experience upward mis-centering or images with a large FOV so that the patient table may be <450 (pixels). However, a user can change the threshold value for the table position. The implementation of the table (or head support) removal method using MatLab software can be found in the Supplementary material.

We evaluated patient images from only one particular CT machine. The algorithm has not been tested on images from other CT machines. A comparison of the values of $D_{w,t}$ and $D_{w,f}$ may be affected by differences in table design and materials for different CT machines. This study was only carried out on chest and head images and has not yet carried out on other parts of the body. We only used adult patients of moderate size; the results may be different for adult obesity patients or pediatric patients. We found that, if it is not possible to calculate $D_{w,f}$ or $D_{w,c}$, the calculation of the water-equivalent diameter value using this method ($D_{w,t}$ and $D_{w,\mathrm{nt}}$) is more accurate than using only patient geometry (i.e. effective diameter, D_{eff}). The difference between $D_{w,f}$ and D_{eff} was up to ±10%[28].

CONCLUSIONS

We proposed a simple method to estimate the water-equivalent diameter from entire CT images without using a ROI ($D_{w,t}$). We found that this method was accurate and differed from the estimate of water-equivalent diameter calculated using a ROI fitted to the patient border ($D_{w,f}$) to within ±5% for all of our head images and most (27 of the 30 patients, 90%) of our thoracic images. We also proposed a simple method for recognizing and removing table (or head support) remnants from patient images. This method was able to recognize and remove table (head support) remnants from all images used. The resulting water-equivalent diameter ($D_{w,\mathrm{nt}}$) was more accurate, to within 5% for all images, whether head or thoracic images.

SUPPLEMENTARY MATERIAL

Supplementary material can be found at *Radiation Protection Dosimetry* online

ACKNOWLEDGMENT

The authors would like to acknowledge Mr. Masdi from Prof. Dr. Margono Hospital for providing images of patients.

FUNDING

This work was supported by Penelitian Dasar Unggulan Perguruan Tinggi (PDUPT), Ministry of Research Technology and Higher Education of the Republic of Indonesia, contract number 532z/I1. C01/PL/2018.

REFERENCES

1. Pearce, M. S. *et al. Radiation exposure from CT scans in childhood and subsequent risk of leukaemia and brain tumours: a retrospective cohort study*. Lancet **380**, 499–505 (2012).
2. Mathews, J. D. *et al. Cancer risk in 680 000 people exposed to computed tomography scans in childhood or*

adolescence: data linkage study of 11 million Australians. BMJ **346**, f2360 (2013).
3. Miglioretti, D. L. *et al*. *Pediatric computed tomography and associated radiation exposure and estimated cancer risk*. JAMA Pediatr. **167**, 700–707 (2013).
4. Brenner, D. J., Elliston, C. D., Hall, E. J. and Berdon, W. E. *Estimated risks of radiation-induced fatal cancer from pediatric CT*. Am. J. Roentgenol. **176**, 289–296 (2001).
5. Brenner, D. J. and Hall, E. J. *Computed tomography—an increasing source of radiation exposure*. N. Engl. J. Med. **357**, 2277–2284 (2007).
6. Voress, M. *The increasing use of CT and its risks*. Radiol. Technol. **79**, 186–190 (2007).
7. Kalra, M. K., Maher, M. M., Toth, T. L., Hamberg, L. M., Blake, M. A., Shepard, J. A. and Saini, S. *Strategies for CT radiation dose optimization*. Radiology **230**, 619–628 (2004).
8. Anam, C., Haryanto, F., Widita, R., Arif, I. and Dougherty, G. *The size-specific dose estimate (SSDE) for truncated computed tomography images*. Radiat. Prot. Dosim. **175**, 313–320 (2017).
9. Boos, J., Lanzman, R. S., Heusch, P., Aissa, J., Schleich, C., Thomas, C., Sawicki, L. M., Antoch, G. and Kröpil, P. *Does body mass index outperform body weight as a surrogate parameter in the calculation of size-specific dose estimates in adult body CT?* Br. J. Radiol. **89**, 20150734 (2016).
10. Martin, C. J. and Huda, W. *Intercomparison of patient CTDI surveys in three countries*. Radiat. Prot. Dosim. **153**, 431–440 (2013).
11. Anam, C., Haryanto, F., Widita, R., Arif, I., Fujibuchi, T., Toyoda, T. and Dougherty, G. *Scatter index measurement using a CT dose profiler*. J. Med. Phys. Biop. **4**, 95–102 (2017).
12. Burton, C. S. and Szczykutowicz, T. P. *Evaluation of AAPM Reports 204 and 220: Estimation of effective diameter, water-equivalent diameter, and ellipticity ratios for chest, abdomen, pelvis, and head CT scans*. J. Appl. Clin. Med. Phys. **19**, 228–238 (2018).
13. Anam, C., Haryanto, F., Widita, R., Arif, I. and Dougherty, G. Automated calculation of water-equivalent diameter (D_W) based on AAPM task group 220. J. Appl. Clin. Med. Phys. **17**, 320–333 (2016).
14. Wu, J., Han, R. and Liu, Y. *Using a somatosensory controller to assess body size for size-specific dose estimates in computed tomography*. BioMed Res. Int. **2018**, 1–7 (2018).
15. Anam, C., Haryanto, F., Widita, R., Arif, I. and Dougherty, G. *The evaluation of the effective diameter (D_{eff}) calculation and its impact on the size-specific dose estimate (SSDE)*. Atom Indones. **43**, 55–60 (2017).
16. Bashier, E. H. and Suliman, I. I. *Multi-slice CT examinations of adult patients at Sudanese hospitals: radiation exposure based on size-specific dose estimates (SSDE)*. Radiol. Med. **123**, 424–431 (2018).
17. Özsoykal, I., Yurt, A. and Akgüngör, K. *Size-specific dose estimates in chest, abdomen, and pelvis CT examinations of pediatric patients*. Diagn. Interv. Radiol. **24**, 243–248 (2018).
18. Fujii, K., McMillan, K., Bostani, M., Cagnon, C. and McNitt-Gray, M. *Patient size–specific analysis of dose indexes from CT lung cancer screening*. Am. J. Radiol. **208**, 1–6 (2017).
19. Sarmento, S., Mendes, B. and Gouvêa, M. *Automatic calculation of patient size metrics in computed tomography: What level of computational accuracy do we need?* J. Appl. Clin. Med. Phys. **19**, 218–227 (2018).
20. Zhang, D., Mihai, G., Barbaras, L. G., Brook, O. R. and Palmer, M. R. *A new method for CT dose estimation by determining patient water equivalent diameter from localizer radiographs: geometric transformation and calibration methods using readily available phantoms*. Med. Phys. **45**, 3371–3378 (2018).
21. American Association of Physicists in Medicine. *Use of water equivalent diameter for calculating patient size and size-specific dose estimates (SSDE) in CT*. Report no 220. College Park, MD: American Association of Physicists in Medicine (2014). Website: www.aapm.org/pubs/reports/RPT_220.pdf (27 October 2015, date last accessed).
22. American Association of Physicists in Medicine. *Size-specific dose estimates (SSDE) in pediatric and adult body CT examinations*. Report no 204. College Park, MD: American Association of Physicists in Medicine (2011). Website: www.aapm.org/pubs/reports/rpt_204.pdf (4 February 2015, date last accessed).
23. Boos, J., Thomas, C., Appel, E. *et al*. *Institutional computed tomography diagnostic reference levels based on water-equivalent diameter and size-specific dose estimates*. J. Radiol. Prot. **38**, 536–548 (2018).
24. Anam, C., Fujibuchi, T., Toyoda, T. *et al*. *A simple method for calibrating pixel values of the CT localizer radiograph for calculating water-equivalent diameter and size-specific dose estimate*. Radiat. Prot. Dosim. **179**, 158–168 (2018).
25. Christner, J. A., Braun, N. N., Jacobsen, M. C., Carter, R. E., Kofler, J. M. and McCollough, C. H. *Size-specific dose estimates for adult patients at CT of the torso*. Radiology **265**, 841–847 (2012).
26. Li, B., Behrman, R. H. and Norbash, A. M. *Comparison of topogram-based body size indices for CT dose consideration and scan protocol optimization*. Med. Phys. **39**, 3456–3465 (2012).
27. Wang, J., Christner, J. A., Duan, Y., Leng, S., Yu, L. and McCollough, C. H. *Attenuation-based estimation of patient size for the purpose of size specific dose estimation in CT. Part II. Implementation on abdomen and thorax phantoms using cross sectional CT images and scanned projection radiograph images*. Med. Phys. **39**, 6772–6778 (2012).
28. Daudelin, A., Medich, D., Andrabi, S. Y. and Martel, C. *Comparison of methods to estimate water-equivalent diameter for calculation of patient dose*. J. Appl. Clin. Med. Phys. **19**, 718–723 (2018).
29. Anam, C., Haryanto, F., Widita, R., Arif, I., Dougherty, G. and McLean, D. *The impact of patient table on size-specific dose estimate (SSDE)*. Australas. Phys. Eng. Sci. Med. **40**, 153–158 (2017).
30. Zhu, Y., Cochoff, S. M. and Sukalac, R. *Automatic patient table removal in CT images*. J. Digit. Imaging **25**, 480–485 (2012).
31. Kim, J., Hu, Y., Eberl, S., Feng, D. and Fulham, M. *A fully automatic table/linen segmentation for fused PET/CT MIP rendering*. J. Nucl. Med. **49**, 387 (2008).
32. http://www.vivoquant.com/cgi-bin/manual.cgi?tools-bedremoval.html (5 November 2018, date last accessed).